Senescent cells expose and secrete an oxidized form of membrane-bound vimentin as revealed by a natural polyreactive antibody

David Frescas[a,1], Christelle M. Roux[a], Semra Aygun-Sunar[a], Anatoli S. Gleiberman[a], Peter Krasnov[a], Oleg V. Kurnasov[b], Evguenia Strom[a], Lauren P. Virtuoso[a], Michelle Wrobel[a], Andrei L. Osterman[b], Marina P. Antoch[c], Vadim Mett[a], Olga B. Chernova[a,1], and Andrei V. Gudkov[a,d,1]

[a]Everon Biosciences, Inc., Buffalo, NY 14263; [b]Infectious and Inflammatory Disease Center, Sanford-Burnham Medical Research Institute, La Jolla, CA 92037; [c]Department of Pharmacology and Therapeutics, Roswell Park Cancer Institute, Buffalo, NY 14263; and [d]Department of Cell Stress Biology, Roswell Park Cancer Institute, Buffalo, NY 14263

Edited by Ruslan Medzhitov, Yale University School of Medicine, New Haven, CT, and approved January 24, 2017 (received for review September 1, 2016)

Studying the phenomenon of cellular senescence has been hindered by the lack of senescence-specific markers. As such, detection of proteins informally associated with senescence accompanies the use of senescence-associated β-galactosidase as a collection of semiselective markers to monitor the presence of senescent cells. To identify novel biomarkers of senescence, we immunized BALB/c mice with senescent mouse lung fibroblasts and screened for antibodies that recognized senescence-associated cell-surface antigens by FACS analysis and a newly developed cell-based ELISA. The majority of antibodies that we isolated, cloned, and sequenced belonged to the IgM isotype of the innate immune system. In-depth characterization of one of these monoclonal, polyreactive natural antibodies, the IgM clone 9H4, revealed its ability to recognize the intermediate filament vimentin. By using 9H4, we observed that senescent primary human fibroblasts express vimentin on their cell surface, and MS analysis revealed a posttranslational modification on cysteine 328 (C328) by the oxidative adduct malondialdehyde (MDA). Moreover, elevated levels of secreted MDA-modified vimentin were detected in the plasma of aged senescence-accelerated mouse prone 8 mice, which are known to have deregulated reactive oxygen species metabolism and accelerated aging. Based on these findings, we hypothesize that humoral innate immunity may recognize senescent cells by the presence of membrane-bound MDA-vimentin, presumably as part of a senescence eradication mechanism that may become impaired with age and result in senescent cell accumulation.

aging | oxidative posttranslational modifications | biomarker | SAMP8 | malondialdehyde

Cellular senescence is a multistep process that halts the proliferation of damaged or dysfunctional cells to restrict the progression of malignancy (1–3). Although senescence serves to constrain aberrant proliferation to counteract cellular transformation, the accumulation of senescent cells over time may play an equally adverse role (4). Secreted proteins produced by senescent cells are collectively referred to as senescence-associated secretory phenotype (SASP) factors (5). These factors include proinflammatory cytokines and chemokines, as well as various growth factors, proteases, extracellular matrix proteins and others (4–6). The accumulation of senescent cells and the accompanied production of SASP have been implicated in tissue dysfunction and overall loss of the regenerative potential of tissues, both of which are observed with aging (7–9). Moreover, the presence of SASP factors has also been shown to induce an epithelial–mesenchyme transition and angiogenesis that supports cancer cell invasiveness (5). Although senescent cells are thought to naturally accumulate in various tissues and organs with age, the mechanisms by which this occurs is not yet fully understood. Evidence that senescent cells are targets of the immune system suggests that the efficiency by which senescent cells are cleared may play a key role in their accumulation (10, 11).

The shortage of markers needed to identify senescent cells and to quantitate their numbers is a major hindrance to studying senescence in vivo and in vitro (12). Currently, the detection of proteins described to be associated with senescence, such as p16, p21, IL-6, γ-H2AX, phosphorylated p38 MAPK, and most recently GATA4, accompanies the use of senescence-associated β-galactosidase (SA-β-Gal) as an assortment of semiselective senescence markers, many of which are additionally involved in many senescence-independent cellular processes (13, 14). Here, we describe our efforts to identify senescence-specific markers (antibodies and their corresponding antigens) by immunizing mice with senescent cells. In this way, we set out to challenge the murine immune system to respond to naturally occurring antigenic substrates: that is, cell-surface immune ligands that can mediate recognition by the immune system (15). Among the dozens of antibody clones that we isolated and screened for immunoreactivity toward senescent cells, many were of the IgM isotype. Germ-line–type IgMs, also termed "natural antibodies," are part of the innate immune system and are the most evolutionarily conserved antibody isotype (16–18). As the earliest isotype to be expressed during immune development, IgMs are thought to have been selected during the evolution of immunity for their contribution to critical immunoregulatory and housekeeping functions, which include clearance of apoptotic cells to prevent inflammation and autoimmunity (19, 20). Intriguingly,

Significance

Understanding the mechanisms underlying the development of senescence and the consequences related to the accumulation of senescent cells is a major focus of ongoing research. Our report shows that senescent cells express a form of oxidized vimentin on their cell surface and that oxidized vimentin is secreted into the blood of senescence-prone senescence-accelerated mouse prone 8 mice. Given the growing evidence that oxidized proteins are involved in the development of human diseases, the detection and monitoring of secreted proteins like malondialdehyde-modified vimentin is certain to become a vital and noninvasive biomarker for studying senescence and monitoring age-related illnesses.

Author contributions: D.F., A.S.G., A.L.O., M.P.A., V.M., O.B.C., and A.V.G. designed research; D.F., C.M.R., S.A.-S., A.S.G., P.K., O.V.K., E.S., L.P.V., M.W., M.P.A., and V.M. performed research; D.F., C.M.R., S.A.-S., A.S.G., P.K., E.S., A.L.O., M.P.A., O.B.C., and A.V.G. analyzed data; and D.F., A.S.G., V.M., and A.V.G. wrote the paper.

Conflict of interest statement: O.B.C. and A.V.G. are cofounders and shareholders of Everon Biosciences, a biotech company that funded this work and owns related intellectual property.

This article is a PNAS Direct Submission.

Freely available online through the PNAS open access option.

[1]To whom correspondence may be addressed. Email: dfrescas@tartiscorp.com, ochernova@tartiscorp.com, or andrei.gudkov@roswellpark.org.

This article contains supporting information online at www.pnas.org/lookup/suppl/doi:10.1073/pnas.1614661114/-/DCSupplemental.

other components of the innate immune system, including natural killer (NK) cells, neutrophils, dendritic cells, and macrophages, functionally contribute to elimination of senescent cells (11, 15, 21). NK cells, for example, have been shown to recognize and eliminate senescent cells after expression of NK receptor ligands, adhesion molecules (intercellular adhesion molecule-1), and death receptors (TRAIL-R and FAS), respectively (10, 11, 15). Moreover, natural IgMs have been shown to play a significant role in the clearance of senescent red blood cells (22).

Ongoing efforts to determine the antigenic targets of our senescence-associated antibodies resulted in the discovery of vimentin on the surface of senescent cells. Vimentin is characteristically known as a cytosolic protein that plays a major role in intermediate filament assembly and function. Nonetheless, vimentin has also been shown to interact with the nucleus and the membranes of cells (23). Using our IgM clone 9H4, we show that vimentin accumulates on the surface of senescent cells, and we demonstrate that senescence-associated cell-surface vimentin is modified by the oxidative adduct malondialdehyde (MDA). These observations are in agreement with previous studies showing that one of the major antigens of natural IgMs are oxidation-associated neo-epitopes, which become distinctively exposed on the cell surface of dysfunctional cells to allow recognition by the immune system (16, 24). MS analysis confirmed the presence of MDA on senescence-associated cell-surface vimentin and identified an oxidation-associated neo-epitope on cysteine 328 (C328). Because the detection of senescence-specific epitopes may support the development of non-invasive clinical tools to identify and monitor age-related diseases linked to the accumulation of senescent cells, we developed a sandwich ELISA using 9H4 to measure secreted modified vimentin in the plasma of the senescence-accelerated mouse prone 8 (SAMP8) mouse model, resulting in the detection of elevated MDA-vimentin levels in SAMP8 mice compared with C57BL/6 mice. Taking these data together, we propose the detection of secreted MDA-modified vimentin as a readout of senescent cells.

Results

Generation of Antibodies Against Senescent Cells. Tissue culture cells have previously been used to immunize mice to generate antibodies to cell-surface antigens (25, 26). To generate antibodies with immunoreactivity toward senescent cells, BALB/c mice were immunized intraperitoneally with syngeneic bleomycin-treated, senescent mouse lung fibroblasts (mLFs) (Fig. S1 *A* and *B*). The induction of antibodies was evaluated via FACS analysis of untreated and bleomycin-treated mLFs following their incubation with serum collected from immunized mice (Fig. S1*C*). Hybridomas were then produced by fusion of splenocytes from selected immunized mice with murine myeloma Sp2/0 cells, and a primary screen of antibodies to compare binding between untreated and senescent mLFs was performed again by FACS (Fig. S1*D*). Antibody clones that showed selective immunoreactivity toward senescent cells were chosen, produced in large scale, isotyped, and their light- and heavy-chain variable regions were sequenced. Isotyping and sequencing showed that the majority of these antibody clones were germ-line–type IgMs (Fig. S2). IgMs, which are often referred to as natural antibodies, are part of the innate immune system (18, 27).

A senescence-associated cell-based ELISA (SACE) assay was developed as a secondary screen to identify those antibodies with highest affinity toward the cell surface of live senescent cells. To generate senescent cells for SACE analysis, normal human primary dermal fibroblasts (NDFs) were treated with 10-Gy irradiation (IR), plated on tissue culture dishes, and allowed to senesce over the course of 2–3 wk (Fig. S3 *A* and *B*). Importantly, cellular viability and cell size (as determined by FACS analysis) of these IR-treated cells was comparable to that of untreated cells (Fig. S3 *A* and *C*). By applying our SACE assay, we observed that several of our IgM antibodies, a subset which are shown in Fig. 1*A*, were capable of discriminating between untreated and IR-treated cells. Notably, the 9H4 antibody clone was particularly proficient at recognizing senescent cells (Fig. 1*A*). Therefore, based on these data, 9H4 was among those chosen for further characterization.

Although natural antibodies like the IgM E06 [an anti-phosphorylcholine (PC) antibody] have been shown to recognize apoptotic cells (28–32), 9H4 failed to recognize Annexin V^+ NDFs undergoing apoptosis following staurosporine treatment (Fig. 1*B* and Fig. S3*D*). Moreover, we found that recognition of senescent cells by the 9H4 antibody was dependent upon the onset of senescence, as observed via a 3-wk-long time-course experiment following IR, and by the antibody concentration used in the SACE assay (Fig. 1 *C* and *D*). Levels of fibroblast surface protein (FSP), a fibroblast surface antigen that was detected using a commercial monoclonal IgM antibody (33), did not show significant differences between untreated and IR-treated cells (Fig. 1*C*). These data substantiate the method of isolating senescence-associated antibodies following immunization with senescent cells, which we independently validated by performing a secondary screen using a modified cell-based ELISA. Furthermore, these efforts led to the identification of the IgM antibody 9H4 as a putative biomarker for recognizing senescent cells.

9H4 Recognizes Vimentin and Oxidative Posttranslational Modifications. To begin to determine the antigenic targets of our 9H4 IgM clone, we performed indirect immunofluorescence and observed that 9H4 colocalized predominantly with the intermediate filament vimentin in PFA-fixed and Triton X-100 permeabilized untreated and IR-treated NDF cells (Fig. 2*A* and Fig. S4*A*). As part of the type III intermediate filament protein family, vimentin is a widely expressed and highly conserved protein that supports cellular integrity and provides resistance against mechanical stress (23). Immunoblotting of whole-cell lysates (WCE) from untreated, bleomycin-treated, and IR-treated NDF cells showed that 9H4 recognized a major band at ~57 kDa, which slightly increased in the lysates of senescent cells (Fig. 2*B*). A less-intense secondary band was also detected at 45 kDa (Fig. 2*B*). Consistent with these data, the molecular mass of vimentin is ~57 kDa, and the levels of vimentin have been shown to increase during senescence in fibroblasts (34). To further confirm that 9H4 recognized vimentin, we performed Western blot analysis using vimentin produced in *Escherichia coli* and observed that 9H4 was capable of detecting the recombinant version of vimentin (Fig. 2*C*). 9H4 was also capable of detecting recombinant vimentin in a sandwich ELISA using a commercial chicken polyclonal anti-vimentin capture antibody (Fig. 2*D*).

IgMs are capable of forming polymers (mostly pentamers with 10 antigen-binding sites) through covalent linkage of disulfide bonds. Consequently, naturally occurring IgMs are inherently polyreactive and among the diverse antigens of natural antibodies are synthetic haptens, nucleotides, polysaccharides, oxidized lipids, and advanced glycation end products (AGEs) (17, 35, 36). To determine if 9H4 exhibited polyreactivity, we performed direct ELISAs using a series of haptens and antigens previously used to characterize IgMs (35). We also included the oxidation-specific adducts MDA and PC, as well as the AGE-associated modification carboxymethyl lysine (CML) conjugated to BSA in this analysis. 9H4 showed immunoreactivity against more than one antigen in the test group, suggesting our IgM clone was indeed polyreactive (Fig. 2*E* and Fig. S4*B*). Interestingly, of the naturally occurring antigens, 9H4 was capable of binding to BSA-conjugated MDA, single-stranded DNA (ssDNA), and to a lesser extent BSA-conjugated CML (Fig. 2*E* and Fig. S4*B*). Unlike the E06 antibody, 9H4 failed to recognize PC-BSA or double-stranded DNA (dsDNA), respectively (Fig. 2*E* and Fig. S4 *B* and *C*). Taken together, these data show that the intermediate filament vimentin and the oxidative posttranslational modifications MDA and CML are antigenic targets of 9H4.

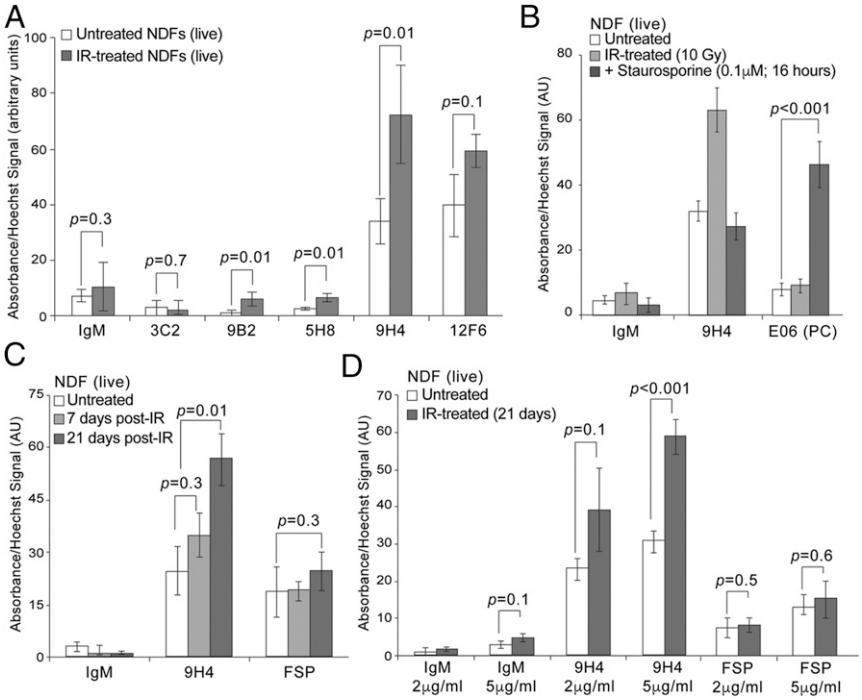

Fig. 1. Generation and isolation of antibodies against senescent cells. (*A*) SACE analysis using IgM clones to detect immunoreactivity toward live senescent NDF cells. An HRP-conjugated IgM-specific secondary antibody was used in conjunction with TMB substrate for colorimetric ELISA reading at an absorbance of 450 nm to detect binding of IgMs to the surface of cells. DNA was stained with cell permeable Hoechst to normalize TMB absorbance values. Values (arbitrary units) and SDs were calculated from triplicates. An unpaired Student's *t* test was used for statistical analysis. (*B*) SACE analysis (as in *A*) using whole-molecule mouse IgM (negative control) or the IgM antibodies 9H4 and E06 to detect immunoreactivity toward live untreated, senescent, or staurosporine-treated (0.1 μM for 16 h) NDF cells. Values (arbitrary units) and SDs were calculated from triplicates. An unpaired Student's *t* test was used for statistical analysis. (*C*) SACE analysis (as in *A*) using whole-molecule mouse IgM (negative control) or the IgM antibodies 9H4 and anti-FSP to detect immunoreactivity toward live senescent NDF cells. Values (arbitrary units) and SDs were calculated from triplicates. An unpaired Student's *t* test was used for statistical analysis. (*D*) SACE analysis (as in *A*) using whole-molecule mouse IgM (negative control) or the IgM antibodies 9H4 and anti-FSP to detect antibody dose-dependency and immunoreactivity toward live senescent NDF cells. Values (arbitrary units) and SDs were calculated from triplicates. An unpaired Student's *t* test was used for statistical analysis.

Enrichment of Vimentin on the Surface of Senescent Cells. In addition to playing a fundamental role as an intermediate filament in cytoskeletal assemblies, vimentin has been shown to associate with the nucleus and cell membranes of various cell types (37–43). Because 9H4 recognizes senescent cells by SACE analysis, which is an assay that requires robust antibody interactions with cell-surface antigens, we performed a cellular fractionation experiment to determine if vimentin was enriched on the surface of senescent NDFs. Immunoblotting of subcellular fractions showed vimentin, as detected by 9H4, resided predominantly in the cytoskeletal fraction of untreated NDFs (Fig. 3*A*). Quantification by band densitometry analysis of immunoblots showed that ∼50% of vimentin is associated with the cytoskeleton (Fig. 3*B*). In senescent cells, however, vimentin was observed to substantially increase in the membrane fraction by at least 20%, which coincided with an equivalent decrease in signal from the cytoskeletal fraction (Fig. 3 *A* and *B*). Notably, the percentage of vimentin associated with the cytoplasm or nucleus did not appear to change between the two conditions (Fig. 3 *A* and *B*).

To further confirm that vimentin was enriched on the membranes of senescent cells, we fractionated cells and performed a pull-down assay with 9H4. Coomassie staining of immunoprecipitated proteins revealed a band at 45 kDa, a band at 57 kDa, and a band between 70 and 100 kDa (Fig. 3*C*). Of these bands, only the 57-kDa band was immunoreactive with both 9H4 and a commercial polyclonal antivimentin antibody (Fig. 3*C*). SACE analysis using this commercial antivimentin antibody confirmed enrichment of vimentin on the surface of senescent cells (Fig. S5*A*). Importantly, fixation and permeabilization of cells with methanol before SACE analysis resulted in the loss of assay specificity, presumably because of intracellular vimentin accessibility by the antibodies (Fig. S5*B*). Next, we performed an ELISA to measure vimentin amounts in membrane lysates and determined that vimentin was ∼four times more abundant on the surface of senescent cells (Fig. S5*C*). The levels of FSP, as anticipated, did not change between conditions (Fig. S5*C*). Finally, we performed indirect immunofluorescence on cells fixed by PFA (not permeabilized), and observed that 9H4 also colocalized predominantly with the intermediate filament vimentin on the cell surface of untreated and IR-treated NDF cells (Fig. 3*D*). Notably, dot-like arrangements of vimentin were observed in untreated NDFs, resembling a pattern previously published (40), the vimentin detected in senescent cells appeared to occupy a larger and more prominent swath of the cell surface (Fig. 3*D*). Enrichment of cell-surface vimentin was correspondingly observed in bleomycin-treated mLFs immunostained with 9H4 (Fig. S5*D*). Taken together, these data demonstrate the enrichment of vimentin on the surface of senescent cells.

Senescence-Associated Cell-Surface Vimentin Is Modified by MDA. Vimentin was previously found to be modified by MDA in the human brain cortex of Alzheimer's patients and by CML in skin fibroblasts isolated from elderly donors and exposed to UV light (44, 45). Given that vimentin is the target of various post-translational modifications that include oxidation (46, 47), we thus examined whether these oxidative adducts were associated with vimentin exposed on the surface of senescent cells. To that end, we performed a combinatorial vimentin IP and time-course experiment. NDF cells were irradiated, allowed to senesce, and harvested at different time points over 21 d, and a commercial polyclonal vimentin antibody was used to nondiscriminately isolate

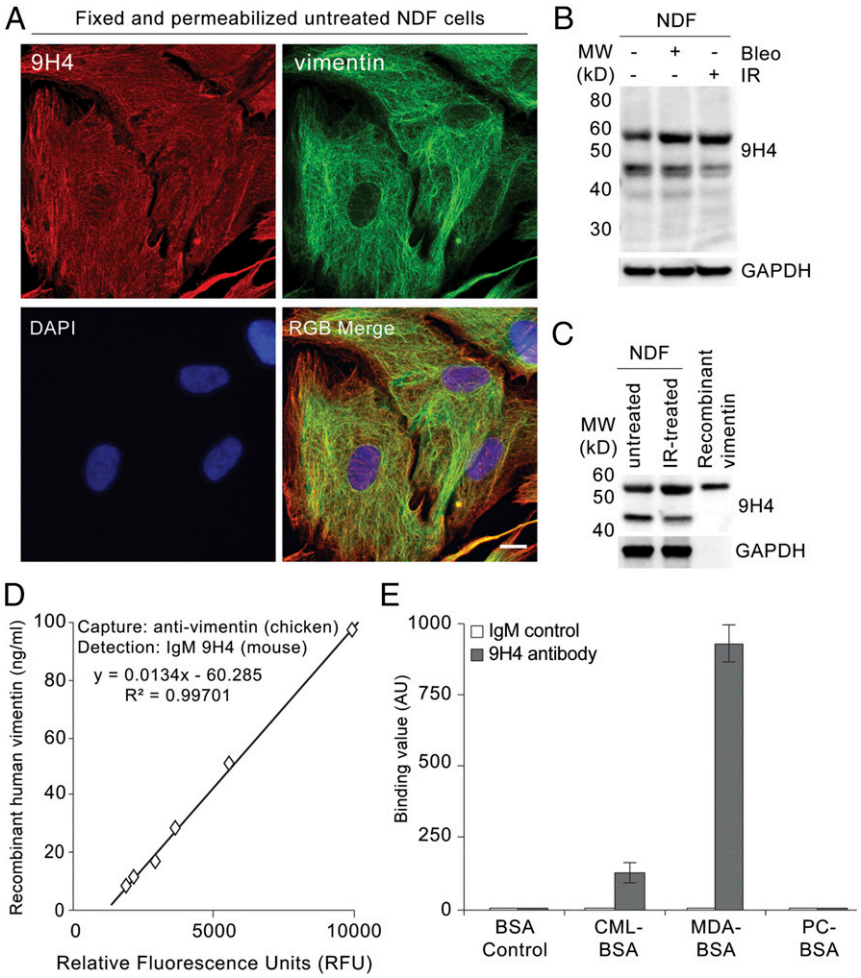

Fig. 2. IgM 9H4 clone recognizes the intermediate filament vimentin. (*A*) Immunofluorescence staining of 2% PFA fixed and Triton X-100 permeabilized untreated NDF cells stained with IgM 9H4 clone (red) and an antivimentin antibody (green). DNA was stained with DAPI (blue). (Scale bar, 5 μm.) (*B*) Immunoblot of WCE from untreated, IR-treated, or bleomycin-treated NDFs using IgM 9H4, as indicated. GAPDH is used as loading control. (*C*) Immunoblot of WCE from untreated or IR-treated NDFs and recombinant human vimentin using IgM 9H4, as indicated. GAPDH is used as loading control. (*D*) Sandwich ELISA measuring increasing levels of recombinant human vimentin. A polyclonal antivimentin (chicken) antibody was used as a capture antibody and IgM 9H4 was used to detect vimentin. (*E*) Polyreactivity of IgM 9H4 or whole-molecule IgM was measured by direct ELISA. Binding value was assessed for each antibody by testing their binding to BSA or the indicated BSA-conjugated haptens. Values (arbitrary units) and SDs were calculated from triplicates. An unpaired Student's *t* test was used for statistical analysis.

all membrane-bound forms of vimentin (i.e., with or without modifications). We observed that MDA-modified vimentin was present in low amounts in untreated NDFs, as detected with an anti-MDA antibody (Fig. 4*A*). Following IR-treatment to induce senescence, we detected a significant increase in the levels of MDA adduction on vimentin (Fig. 4*A*). Moreover, vimentin isolated from senescent cells also appeared to be modified by CML, albeit to a lesser extent, whereas vimentin did not appear to be modified by PC (Fig. S6*A*). Importantly, we also observed MDA-modified vimentin in NDFs transduced with HRas G12V (oncogene-induced senescent cells) (Fig. 4*B* and Fig. S6*B*) and late-passage NDFs (containing a majority of replicatively senescent cells) (Fig. 4*C* and Fig. S6*C*).

To identify amino acids potentially modified on vimentin, we generated protein extracts from the plasma membranes of IR-treated NDFs through a sucrose gradient centrifugation procedure and performed an immunoprecipitation (IP) using the same commercial polyclonal antivimentin antibody used in Fig. 4*A*. Coomassie staining of immunoprecipitated proteins revealed bands at 45 kDa and at ∼57 kDa (Fig. 4*D*). Tryptic digestion of the 57-kDa band was performed, and LC-MS/MS analysis was conducted. MS analysis identified 43 peptide sequences of high confidence, all of which matched the human vimentin amino acid sequence and spanned 71% of the protein (Fig. 4*D*). Vimentin peptides were unbiasedly analyzed for all posttranslational modifications and specifically for MDA, CML, and PC adducts. Vimentin from senescent NDF cells was found to be modified by MDA at its single cysteine residue (C328), as indicated by a mass change of +54.0105 Da (Fig. 4*E*). C328 is located at the C-terminal end of the protein and is evolutionarily conserved (Fig. 4 *F* and *G* and Fig. S6*D*). Interestingly, C328 has been shown to be required for proper function of vimentin in human cells under normal and oxidative conditions (48). The oxidative adduct aldehyde 4-hydroxynonenal (HNE) has been previously shown to modify vimentin at C328 (49); however, an HNE modification at C328 was not identified in our proteomic screen. Moreover, despite detecting CML adducts on senescence-associated cell-surface vimentin via IP-Western (Fig. S6*A*), our proteomic screen failed to identify the location of CML modifications. As anticipated based on pull-down assays, PC modifications on vimentin were not identified.

Senescence-Associated Cell-Surface Vimentin Is Secreted into the Extracellular Environment. Inflammation is considered to be a major consequence of SASP, which proposes that senescent fibroblasts are primed to become proinflammatory cells. Despite

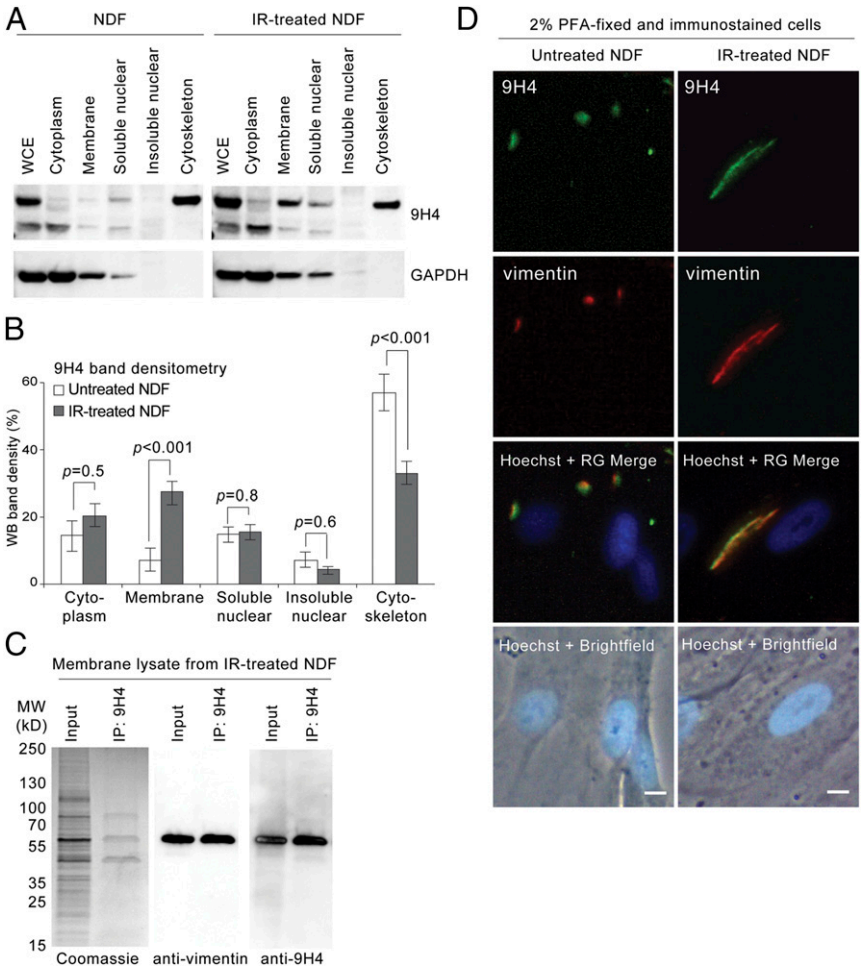

Fig. 3. Oxidized cell-surface vimentin in senescent cells. (*A*) Immunoblot of WCE and cellular fractions (as indicated) from untreated or IR-treated NDFs using IgM 9H4. GAPDH is used as loading control. (*B*) Densitometry analysis of immunoblots (as in *A*) using ImageJ software. Averages are from three independent experiments and SDs were calculated from an unpaired Student's *t* test. (*C*) Isolated membrane lysates from IR-treated NDFs were immunoprecipitated with IgM 9H4. Immunocomplexes were probed for vimentin using an antivimentin antibody and 9H4. (*D*) Immunofluorescence staining of 2% PFA fixed untreated (*Left*) or IR-treated (*Right*) NDF cells stained with IgM 9H4 clone (red) and an antivimentin antibody (green). DNA was stained with live-cell permeable Hoechst (blue). (Scale bar, 5 μm.)

lacking a secretory signal sequence, vimentin is externalized on the cell surface and secreted in various physiological conditions that involve induction of proinflammatory signals, suggesting a possible phenotypic connection to SASP (42, 43, 50, 51). We therefore sought to measure secreted vimentin using our polyreactive 9H4 antibody as a potential readout of senescent cells in vitro and in vivo. To that end, we developed a sandwich ELISA using a recombinant IgG version of our mouse IgM 9H4 antibody. This recombinant rabbit IgG 9H4 antibody was proficient in recognizing vimentin by Western blot analysis and via sandwich ELISA, and continued to be polyreactive toward BSA-conjugated MDA and to a lesser extent BSA-conjugated CML (Fig. S7 *A*–*C*). To determine if senescent cells secrete vimentin, we filtered and concentrated conditioned medium from untreated and IR-treated NDF cells and performed our 9H4–vimentin sandwich ELISA. Vimentin levels were detected to be more than two times higher in the conditioned media collected from IR-treated cells than from control NDFs (Fig. S8*A*). Next, we applied our sandwich ELISA to measure the levels of secreted vimentin in vivo by collecting plasma from mice. For these studies, we used the SAMP8 mouse, which is a naturally occurring accelerated aging model that has been extensively used to study a wide range of age-associated degenerative disorders, including immune dysfunction, osteoporosis and characteristic learning, memory deficits, and brain atrophy (52–59). SAMP8 mice suffer from an increase in cellular oxidative damage and excessive production of reactive oxygen species that results in the progression of cellular senescence (as monitored via an increase in SA-β-Gal positivity) and elevated levels of MDA with age (52, 53). Applying our 9H4-vimentin ELISA, we detected vimentin in the plasma of 35-wk-old SAMP8 mice (Fig. S8*B*). Importantly, a sandwich ELISA designed to directly detect MDA-modified vimentin (using a commercially available anti-MDA antibody for detection) showed a comparable readout pattern compared with the levels of vimentin (as detected with 9H4), suggesting 9H4 was detecting MDA-modified vimentin (Fig. S8*C*). To determine the amount of MDA-modified vimentin in the plasma of SAMP8 mice (in comparison with total vimentin), we immunodepleted MDA-bound proteins from plasma samples using an anti-MDA antibody and performed an immunoblot with remaining plasma proteins. Immunodepletion of MDA-bound proteins resulted in the elimination of all detectable vimentin, suggesting the majority of vimentin in the plasma of SAMP8 is modified by MDA (Fig. S8*D*). Based on these data, we propose the detection of secreted MDA-modified vimentin is a readout of senescent cells.

MDA-Vimentin Levels Inversely Correlate with IgM Levels Against MDA and Vimentin. To determine if the levels of MDA-modified vimentin change with age in SAMP8 mice compared with C57BL6

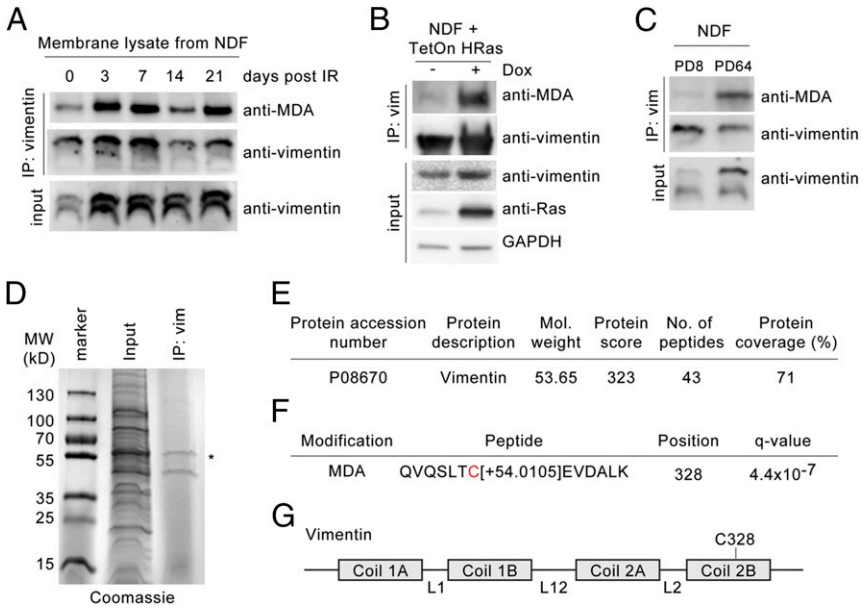

Fig. 4. C328 in vimentin is modified by MDA. (*A*) Isolated membrane lysates from untreated and IR-treated NDFs (3, 7, 14, and 21 d post-IR, respectively) were immunoprecipitated with antivimentin antibody. Immunocomplexes were probed using antibodies against vimentin and MDA (as indicated). (*B*) Isolated membrane lysates from NDF cells transduced with Tet-inducible HRas G12V in the presence or absence of doxycycline (14-d postinduction) were immunoprecipitated with a commercial antivimentin antibody. Immunocomplexes were probed with indicated antibodies, respectively. (*C*) Isolated membrane lysates from early (8 PD) and late (64 PD) passage NDFs were immunoprecipitated with a commercial antivimentin antibody. Immunocomplexes were probed for vimentin and MDA, respectively. (*D*) Plasma membrane lysates from IR-treated NDFs were immunoprecipitated with an antivimentin antibody for MS analysis. Immunocomplexes were highlighted using Coomassie gel staining. An asterisk indicates vimentin at ∼57 kDa. (*E*) Summary of human vimentin peptides identified by nanoCL-electrospray ionization (ESI) MS/MS analysis. (*F*) Type and location of oxidized posttranslational modifications identified on human vimentin by nanoCL-ESI-MS/MS analysis. (*G*) Schematic of human vimentin with major structural components. Location of C328 in the Coil 2B region is shown.

(a commonly used inbred, wild-type laboratory mouse strain), we collected plasma from age-matched, 35- and 54-wk-old SAMP8 and C57BL6 mice, respectively, and performed our 9H4-vimentin ELISA. Elevated levels of MDA-vimentin in the plasma of SAMP8 mice were detected to be higher at 35 and 54 wk of age compared with age-matched C57BL/6 animals (Fig. 5*A*). These findings are in agreement with the observation of elevated levels of oxidative stress markers, including MDA, detected in the plasma of aged SAMP8 mice (53, 55). Several studies have shown associations between the levels of IgMs against oxidized LDL, the presence of oxidized LDL, and diseased states, including cardiovascular disease (60–65); thus, we measured the levels of total IgMs and IgMs against vimentin and MDA in our aged cohorts of SAMP8 and C57BL/6 mice. The levels of IgMs in the plasma of 35- and 54-wk-old C57BL/6 mice slightly increased with age (Fig. S9*A*), as reported for this strain (66), whereas IgMs against vimentin and MDA remained statistically similar in the different age groups (Fig. S9 *B* and *C*). Plasma IgM levels were similarly observed to increase with age in SAMP8 mice (Fig. 5*B*); however, the levels of IgMs against vimentin and MDA decreased with age in these mice (Fig. 5 *C* and *D*). These data suggest that the proficiency by which senescent cells are recognized and eradicated by the innate immune system: that is, via the presence of IgMs against oxidized proteins like MDA-vimentin, may play a crucial role in their accumulation with age.

Discussion

Understanding the mechanisms underlying the development of senescence and the consequences related to the accumulation of senescent cells continues to be a major focus of ongoing research. One of the most challenging aspects of studying such a diverse and multistep process is the lack of clear senescence-specific markers that could be used to identify senescent cells directly or to detect the presence of senescence cells in vivo. To that end, one major goal of our work was the generation of antibodies against senescent cells. This was accomplished by immunizing mice with senescent mLFs. Previous attempts to use cultured cells to immunize mice have been effective in generating antibodies to cell-surface antigens. For example, immunization of mice using cultured malignant prostate cells resulted in the isolation of the PR-1 antibody, which recognizes an antigen present on adenocarcinomas of the prostate (25). Similarly, the FSP antibody that was used throughout this study was derived from mice that were immunized with human thymic fibroblasts (67).

Among the antibody clones that were screened by FACS and then by SACE for immunoreactivity toward senescent cells, a majority emerged as germ-line–encoded, monoclonal IgMs. Notably, the PR-1 and FSP antibodies isolated following immunization with cultured cells are also IgMs (25, 67). Germ-line–encoded IgM antibodies or natural antibodies are part of the innate immune system and appear without immunogenic challenge. A phenotypically distinct subset of B cells (B-1 cells) are responsible for producing natural IgMs in mice, and emerging data suggest the existence of a similar human B-cell counterpart (17, 68, 69). In addition to IgMs recognizing a wide range of microbial and viral components, natural antibodies contribute to immune homeostasis and perform housekeeping functions that include the recognition and removal of apoptotic cells (70). Future studies will need to be conducted to determine if the innate immune system plays a major role in the targeting and clearance of senescent cells.

A major function of the innate immune system is the clearance of apoptotic and damaged cells (10, 11, 21, 71–74). As such, apoptotic cells have been shown to preferentially express or expose novel cell-surface antigens (neo-epitopes or "eat me" signals) that can be recognized by IgMs to initiate phagocytosis by macrophages. The most widely characterized naturally occurring antibody E06 (also known as T15) has the capacity to recognize PC-containing antigens, such as oxidized LDL, which serve as an

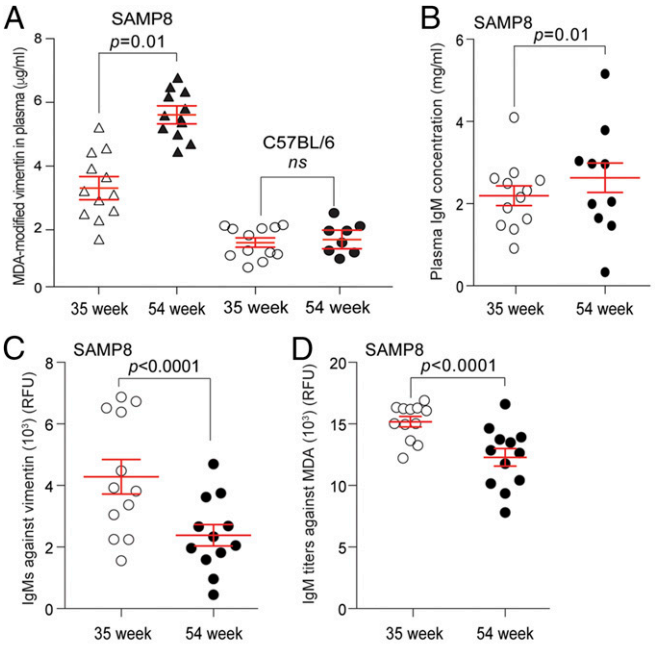

Fig. 5. SAMP8 mice have elevated levels of oxidized vimentin. (*A*) Levels of vimentin from the plasma of 35- and 54-wk-old SAMP8 and C57BL/6 mice were measured using a vimentin-9H4 sandwich ELISA. Sandwich ELISA was developed by using a polyclonal antivimentin (chicken) antibody as a capture antibody and a recombinant IgG 9H4 (rabbit) to detect vimentin. Mean and SEM is shown. An unpaired Student's *t* test was used for statistical analysis. (*B*) Total IgM concentrations collected from the plasma of SAMP8 mice at 35 and 54 wk. Bars represent the median value for each group. (*C*) Levels of IgMs against vimentin in 35- and 54-wk-old SAMP8 mice were determined by ELISA. Bars represent the median value for each group. (*D*) Levels of IgMs against MDA in 35- and 54-wk-old SAMP8 mice were determined by ELISA. Bars represent the median value for each group.

"eat me" signal on the surface of apoptotic cells (29, 61). In our studies, E06 failed to recognize senescent cells, reinforcing the notion of a distinct phenotypic difference between apoptotic and senescent cells. Unlike E06, one of the antibodies that we isolated in our screen, the IgM 9H4, exhibited robust immunoreactivity toward senescent cells and uncovered the presence of the intermediate filament vimentin on the surface of senescent cells. Intriguingly, a number of neo-epitopes are modified intracellular proteins that become exposed on the cell surface, as shown here with vimentin in the context of cellular senescence. The increased presence of MDA-modified vimentin on the surface of senescent cells may indeed serve as an "eat me" signal to immunocytes, as vimentin has been detected on the surface of apoptotic neutrophils (43, 75) and T cells (76), which ultimately leads to phagocytosis by macrophages. Moreover, another study has suggested that cell-surface vimentin present on neighboring cells may interact with radiation induced O-GlcNAc–modified proteins from apoptotic cells to initiate their engulfment by macrophages (77).

Given that germ-line–encoded IgMs have been demonstrated to be polyreactive and may recognize oxidation-associated epitopes (30, 78), we tested 9H4 for reactivity toward synthetic and natural antigens, and we determined that 9H4 recognized MDA alongside vimentin. Interestingly, up to 80% of natural antibodies are thought to be polyreactive; however, the innate ability of these IgMs to recognize multiple, distinct antigens is not clear (35). One hypothesis is that certain ligands may position differently in subsites within the antibody combining site, whereas another possibility is that cross-reacting antigens might share similar epitopes that are capable of recognizing one particular antibody. Notably, unique gene combinations are unlikely to account for IgM polyreactivity (79). Moreover, although 9H4 is proficient in recognizing MDA linked to BSA when tested via ELISA, 9H4 appeared to have greater avidity for vimentin compared with other MDA-linked molecules when denatured proteins are probed via Western blot. A similar result is observed with E06, which recognizes the phosphocholine head-group of oxidized phospholipids that are present in oxidized LDL and BSA-conjugated PC (29, 61). Nevertheless, when E06 is used for Western blot analysis, the antibody recognizes a band of oxidized LDL without highlighting other PC-modified proteins (80).

To determine if vimentin was modified by MDA oxidation, we performed IP-Western studies and demonstrated the presence of MDA on senescence-associated cell-surface vimentin, and LC-MS/MS analysis revealed the addition of MDA on C328. C328 in human vimentin has been shown to be the target of electrophilic lipids that include cyclopentenone prostaglandins (cyPG), which are reactive lipids that are generated under conditions of inflammation and oxidative stress (49, 81, 82). C328 is also subject to covalent addition of the reactive aldehyde HNE, which is similar to MDA (48). CML was previously shown to modify lysines in the exposed linker regions of vimentin after UV treatment (44), and although we detected CML-modified vimentin by IP-Western, our proteomic screen failed to identify the location of these modifications. Importantly, at the cellular level, the modification of vimentin by these oxidation-associated modifications (cyPG, HNE, and CML) has been shown to result in the disruption of the intermediate filament network and the generation of intracellular aggresomes (44, 48, 82).

Detection of vimentin is currently being explored as a biomarker in cancer (41, 83–85), and ongoing studies are currently being conducted to correlate the presence of oxidized proteins, like oxidized LDL to aging and organismal frailty (86, 87). Here, we have developed a sandwich ELISA to detect secreted MDA-modified vimentin using our 9H4 antibody in the context of profiling cellular senescence in vitro and in vivo. Several studies have used the senescence associated mouse SAMP8 to study and monitor aging phenotypes related to elevated levels of oxidative stress, including Alzheimer's disease (52). Whole-exome sequencing of SAMP8 mice revealed deleterious mutations in the disease-causing genes *Ogg1* and *Mbd4* (88). OGG1 (8-oxoguanine glycosylase) is a DNA glycosylate that repairs 8-hydroxyguanine (oh8Gua), a highly mutagenic oxidative DNA damage (89–91), and methyl-CpG binding domain 4 (Mbd4) is a DNA glycosylate involved in DNA demethylation via the pathway (92, 93). BubR1-insufficient mice have similarly been used to study accelerated aging and senescence that results from chronic DNA damage signaling (94, 95).

We applied our 9H4 vimentin-based ELISA to measure vimentin in the plasma of SAMP8 mice and showed SAMP8 mice have elevated MDA-modified vimentin compared with a commonly used mouse model (C57BL/6). We also showed that the levels of MDA-modified vimentin increased as SAMP8 mice age, and this increase was coupled to a decrease in IgMs against vimentin and MDA. Athough MDA-modified vimentin was previously identified in the brain cortex of Alzheimer's patients via a proteomic screen of MDA-oxidized proteins (45), astrocytes in the brain demonstrate age-related changes that resemble those of the SASP, including expression of several cytokines, accumulation of proteotoxic aggregates, and elevated levels of vimentin (96). Nonetheless, the accumulation of MDA-modified vimentin detected in SAMP8 mice may also reflect senescence-independent cellular changes in response to DNA-damage signaling constitutively occurring in this mouse strain (97). Based on these data, we propose the detection of secreted MDA-modified vimentin as a product and readout of senescent cells. Given the growing evidence that oxidized proteins are involved in the development of human disease, the detection and monitoring of secreted proteins like oxidized vimentin is certain to become a vital and noninvasive biomarker for monitoring age-related illnesses (36, 86, 87, 98, 99).

Materials and Methods

Animals. BALB/c (National Cancer Institute–Frederick Cancer Research and Development Center, Frederick, MD), C57BL/6J (Jackson Laboratories), and SAMP8 (Envigo) mice were provided a commercial rodent diet (5% 7012 Teklad LM-485 Mouse/Rat Sterilized Diet, Harlan) and sterile drinking water ad libitum. All of the animals were confined to a limited-access facility with environmentally controlled housing conditions maintained at 18–26 °C, 30–70% air humidity, 12-h light/dark cycle. The animals were housed in microisolation cages under pathogen-free conditions. Animal use in these experiments was approved under Institutional Animal Care and Use Committee at the Roswell Park Cancer Institute.

Cultured Primary Cells. Primary mLFs were isolated based on previously published protocols (100–104). For bleomycin treatment to induce senescence, mLFs were plated at a density of 1.5×10^5 per 10-cm plate and cultured for 72–96 h. Then, 5 mL of medium [DMEM supplemented with 10% (vol/vol) FBS and 10 U/mL Benzonase] was removed and replaced with an equal volume of fresh medium supplemented with a 2× concentration of bleomycin for a final concentration of 5 μg/mL for 72 h at 37 °C and 5% CO_2. Bleomycin-containing medium was removed and replaced with 10 mL of fresh medium and the plates were returned to the incubator for at least 10-d posttreatment before the collection of senescent cells. The percentage of senescent mLFs was determined by SA-β-Gal assay. Senescent mLFs were collected from the plates using TrypLE Express (ThermoFisher Scientific). Human NDFs were purchased from AllCells and maintained in DMEM supplemented with 10% (vol/vol) FBS serum, 100 units/mL of penicillin, 100 μg/mL of streptomycin, and 2 mM L-Glutamine. NDFs were cultured at 37 °C in a 5% CO_2 incubator. To propagate NDF cells, cells were washed once with PBS and trypsin/EDTA was added to detach cells from the tissue-culture dish surface. To stop the Trypsin/EDTA reaction, culture medium was added and cells were resuspended. Resuspended cells were counted and the viability measured using the automated cell counter NC-3000 and Via1 cassettes (Chemometec) according to the manufacturer's protocol. To induce senescence by IR, NDFs were grown to confluence and serum-starved for 48 h before being subjected to 10 Gy IR, as previously reported (105). IR-treated cells were plated and allowed to senesce for 2–3 wk, depending on experimental plans. To induce senescence by bleomycin, bleomycin (15 μg/mL) was added to NDF cells for 48 h, and bleomycin-treated cells were harvested for analysis 14 d posttreatment, as previously reported (106). Overexpression of HRas 612V was previously reported to induce oncogenic cellular senescence (citation). Thus, we introduced a doxycycline-regulated mutant H-Ras G12V into NDF cells. A Lenti-X TET-inducible system was used for inducible expression of V5-tagged HRas G12V (Clontech). To transduce NDFs, cells were incubated in complete medium containing lentivirus and 8 μg/mL polybrene for 6 h. Lentivirus-containing medium was replaced with fresh medium, and the next day, transduced NDFs were selected with 1 μg/mL of puromycin and 600 μg/mL geneticin. To induce expression of HRas G12V, 1 μg/mL of doxycycline was added to these cells for 14 d, and the percentage of senescent cells was determined by SA-β-Gal assay. To harvest proliferating and senescent cells for experimental analysis, TrypLE Express was used to detach cells from the tissue-culture dishes to prevent disruption of cell-surface proteins. Annexin V assay was performed using the NC-3000 instrument according to the manufacturer protocol (Chemometec, Application note 3017).

Generation of Antibodies. Six-week-old BALB/c female mice were immunized intraperitoneally with 1.0×10^6 syngeneic bleomycin-induced senescent mLFs. Two weeks after immunization, two subsequent booster injections were given at 3-wk intervals. Induction of senescent cell-specific antibodies was evaluated through FACS analysis of proliferating cells versus senescent cells following their incubation with serum collected from immunized mice. To obtain the preimmune control serum, mice were bled from the retro-orbital plexus before immunization. Splenocytes were collected from immunized mice and fused with Sp2/0 mouse myeloma cells (cultured in DMEM/F-12) supplemented with 10% (vol/vol) FBS, 1 mM sodium pyruvate, 10 mM Hepes buffer, 1× nonessential amino acids, 1× glutamax, 1× 2-mercaptoethanol, and 100 U/mL penicillin/streptomycin to generate antibody-producing hybridomas. Ten to 14 d after fusion, supernatants from 96-well plates containing hybridoma colonies were removed and applied to primary screening by FACS analysis. Hybridoma supernatants were incubated with Balb/C mLFs (proliferating or senescent) at 4 °C for 30 min. Samples were washed with 3 mL of Phosphate Azide Buffer (PBS with 0.5% BSA and 0.05% sodium azide) and then centrifuged at 500 × *g* for 5 min. Cell pellets were resuspended in 100 μL of buffer and incubated with goat anti-mouse IgG, F(ab′)2-PE at 4 °C for 30 min. Notably, anti-IgG, F(ab′)2 antibodies react with the F(ab′)2/Fab portion of IgG (i.e., the light chain) and are thus not specific for IgG. As a result, anti-IgG, F(ab′)2 antibodies react with other Ig classes (IgA, IgM, IgD, and IgE) sharing the same light chains. After washing and centrifugation, pellets were resuspended in 120 μL of buffer and analyzed by LSRFortessa Cytometer at RPCI Flow Cytometry Resource Facility. Hybridomas were adapted to serum-free medium (supplemented with 1× glutamax, 1× NEEA, 1× AA, 1× Na pyruvate, and 10 mM Hepes; Gibco) and cultured in two-compartment Bioreactor CELLine flasks for large-scale production. Antibody containing medium was harvested on days 14 and 21 and following the centrifugation of the supernatant, and monoclonal IgMs were purified on affinity column chromatography using a HiTrap IgM Purification HP column (GE Healthcare) according to the manufacturer's instructions. Buffer used to elute antibody was exchanged using Zeba Spin Desalting column (ThermoFisher Scientific), and the concentration of the antibodies were determined using a Pierce BCA protein assay kit (ThermoFisher Scientific).

SACE. A 96-well plate was coated with 0.1% gelatin (ThermoFisher Scientific) in PBS for 2 h before cell seeding. NDFs were lifted using TrypLE Express, counted and 75,000 cells (untreated and IR-treated NDFs) were seeded per well in a 100 μL volume. The next day, cells were carefully washed with PBS containing 1 mM $CaCl_2$ and 1 mM $MgCl_2$. Cells were incubated with blocking buffer (2% heat-inactivated goat serum in PBS) for 30 min on ice. After incubation, blocking solution was removed. Primary antibodies were diluted in blocking solution and added to each well in triplicate, and mouse IgM whole molecule (Rockland) served as a negative control. Additional control wells were filled with blocking solution minus primary antibodies. After a 60-min incubation on ice, solutions containing primary antibodies were removed and replaced with PBS to wash. Goat anti-mouse μ-specific IgM secondary antibody (HRP-conjugated; ThermoFisher Scientific) or a goat anti-rabbit IgA+IgG (H+L) (HRP-conjugated) secondary antibody were diluted in blocking solution and added to each well. After a 60-min incubation on ice, solution was removed and replaced with PBS to wash. PBS containing Hoechst was added for 5–10 min to label DNA. Cells were washed twice, and Hoechst signal was read with an Infinite M1000 PRO microplate reader (Tecan). Signal from Hoechst staining was used to detect cell numbers and to normalize 3,3′,5,5′-Tetramethylbenzidine (TMB) values. Next, 1-Step Ultra TMB-ELISA Substrate Solution (Fisher Scientific) was added to cells and plate was read over a 30-min time period. To assay specificity, fixation and permeabilization of cells with methanol was performed before SACE analysis (107). Prism 6 (GraphPad) and Excel (Microsoft) were used to process and graph data.

Antibody Binding to Haptens and DNA by ELISA. BSA-conjugated antigens [DNP-BSA (2,4-dinitrophenyl), Fluorescein-BSA, NIP-BSA (4-hydroxy-3-iodo-5-nitrophenylacetyl), NP-BSA (Ratio > 20) (4-hydroxy-3-nitrophenylacetyl), PC-BSA (phosphorylcholine), and TNP-BSA (2,4,6-trinitrophenyl) (Biosearch Technologies); CML-BSA (carboxymethyl lysine), and MDA-BSA (malonaldehyde) (MyBiosource)] were serially diluted from 1 μg/mL in PBS to 0.0039 μg/mL. Nunc Maxisorp 96-well plates were coated with 50 μL of each concentration and incubated overnight at 4 °C. Nunc Maxisorp plates coated with ssDNA (Sigma) or dsDNA (Sigma) from calf thymus were incubated overnight at 37 °C. After three washes with PBS containing 0.05% Tween-20, plates were incubated for 1 h at room temperature with 80 μL PBS and 1% BSA as a blocking reagent. In the meantime, antibodies were diluted to a final concentration of 10 μg/mL in PBS with 1% BSA. After three washes, 50 μL of each antibody was added to wells and incubated for 2 h at room temperature. The same volume of HRP-conjugated anti-IgM (1:3,000) or -IgG (1:1,500) antibodies was added after three washes and incubated for 1 h. After five washes, colorimetric substrate TMB was added and absorbance was read at 650 nm after 30 min. Prism 6 (GraphPad) and Excel (Microsoft) were used to process and graph data.

Sandwich ELISA for Detection of Vimentin. Nunc Maxisorp Black 96-well plates (Thermo Scientific) were coated with 1.5 μg/mL of chicken polyclonal anti-vimentin (Biolegend) and incubated overnight at 4 °C. Plates were washed twice with Wash Buffer (PBS with 0.05% Tween-20) and blocked for 1 h at room temperature with PBS plus 1% BSA (Blocker BSA in PBS, Fisher Scientific). For the vimentin standard, human recombinant vimentin (Abcam, ab73843) was serially diluted from 1 μg/mL in PBS to 0.0039 μg/mL, added to the plate, and incubated for 1 h at room temperature. Blood was collected from the saphenous vein (50 μL) of mice into heparinized collection vials (Sarstedt), and plasma was obtained following centrifugation at 10,000 × *g* for 7 min at 4 °C. Experimental samples were serially diluted and added to the assay plate. After a 1-h incubation at room temperature, plates were washed twice with Wash Buffer (PBS with 0.05% Tween-20) and primary antibodies were added in blocking buffer for 1 h at room temperature (mouse IgM 9H4; rabbit IgG 9H4; rabbit anti-MDA antibody; Abcam,

ab6463). Plates were washed twice with Wash Buffer (PBS with 0.05% Tween-20) and the secondary antibodies Goat anti-mouse μ-specific IgM secondary antibody (HRP-conjugated; ThermoFisher Scientific) (for IgM 9H4) or peroxidase-conjugated AffiniPure Goat Anti-Rabbit IgG (Rockland) were added in blocking buffer for 1 h at room temperature. Plates were then washed five times and peroxidase fluorogenic substrate (Quanta Blu, ThermoFisher Scientific) was added and fluorescence (excitation 320 nm, emission 420 nm) was read every 10 min for 40 min. To measure secreted vimentin in conditioned media, complete media containing 10% FBS from untreated or IR-treated (14-d post-IR) NDF cells was removed and cells were washed twice with PBS. Serum-free DMEM containing 100 units/mL of penicillin, 100 μg/mL of streptomycin, and 2 mM L-glutamine was added to cells, and NDFs were cultured at 37 °C in a 5% CO_2 incubator for 72 h, as described previously (108). After 72 h, conditioned media was collected, filtered (0.22 μm; EMD Millipore) and concentrated using Amicon Ultra centrifugal filters with a 3-kDa molecular weight cut-off (Merck Millipore). Prism 6 (GraphPad), and Excel (Microsoft) were used to process and graph data.

Immunodepletion of MDA-Vimentin from SAMP8 Plasma. Plasma from SAMP8 mice was collected and incubated with a rabbit polyclonal anti-MDA antibody (Abcam, ab6463) for 1 h at 4 °C. Protein G Sepharose beads (ThermoFisher Scientific) were added for 1 h at 4 °C to pull-down MDA-bound proteins. Sepharose beads were pelleted by centrifugation, and the MDA-immunodepleted supernatant was collected and resuspended in sample buffer. Samples were loaded on a Mini-Protean TGX 4–12% Gradient SDS/PAGE gel (Bio-Rad) and electrophoresed at 100 V. The proteins were then transferred to nitrocellulose membranes in transfer buffer (25 mM Tris, 0.192 M glycine, and 20% methanol) using Trans-Blot Turbo transfer system (Bio-Rad). After blocking for 30 min at room temperature with 5% nonfat dry milk in TBS-T (TBS containing 0.1% Tween 20), membranes were incubated in TBS-T for 1 h at room temperature with a rabbit polyclonal antivimentin antibody (Abcam, ab45939). A goat anti-rabbit IgA+IgG (H+L) HRP-conjugated antibody (ThermoFisher Scientific) was used to detect rabbit-derived antibodies. Following incubation with secondary antibodies, blots were washed thoroughly with TBS-T, incubated with SuperSignal West Dura chemiluminescent peroxidase substrate (Thermo Scientific) and exposed using FluorChem E System: Protein Simple.

Determination of IgM Titers in Plasma Samples. Antibody titers from plasma samples were determined by a sandwich ELISA. Nunc Maxisorp black plates were coated with Affinipure goat anti-mouse IgM diluted 1:1,000 in PBS. After an overnight incubation at 4 °C, the plates were washed three times with PBS-T (PBS + 0.05% Tween-20). Plates were then blocked with assay buffer (PBS-T + 10% FBS) for 1 h at room temperature and washed once. Plasma samples were serially diluted in assay buffer and added in duplicate and incubated for 2 h at room temperature. Following three washes, peroxidase-conjugated rabbit anti-mouse IgM antibodies were added and incubated for 1 h at room temperature. Plates were washed five times and peroxidase fluorogenic substrate (Quanta Blu) was added and fluorescence (excitation 320 nm, emission 420 nm) was read after 40 min with an Infinite M1000 PRO microplate reader (Tecan). IgM titers were calculated from the standard curve generated with using IgM whole molecule (Rockland). Prism 6 (GraphPad) and Excel (Microsoft) were used to process and graph data.

Determination of IgM Titers to Vimentin and MDA. Nunc Maxisorp black plates were coated with human recombinant vimentin (Abcam, ab73843) or BSA-conjugated antigens (PC-BSA and CML-BSA and MDA-BSA; MyBiosource) diluted in PBS, and incubated overnight at 4 °C. After three washes with PBS with 0.05% Tween-20, plates were incubated for 1 h at room temperature and 1% BSA as a blocking reagent. After three washes, the plasma samples were diluted to 1:500 and each sample was added to wells and incubated for 2 h at room temperature. HRP-conjugated anti-IgM antibody was added after three washes and incubated for 1 h. Following five washes, fluorogenic substrate was added and fluorescence was read after 30 min with an Infinite M1000 PRO microplate reader (Tecan). Prism 6 (GraphPad) and Excel (Microsoft) were used to process and graph data.

ACKNOWLEDGMENTS. We thank Alexandre Rosa Campos at The Sanford-Burnham Medical Research Institute for assistance in performing mass spectrometry analysis; Brandon Hall for thought-provoking discussions and critical reading of the manuscript; and Vitaly Balan for providing valuable research materials. This work was partially funded by a research contract from Everon Biosciences to Roswell Park Cancer Institute (A.V.G. Principle Investigator).

1. Hayflick L, Moorhead PS (1961) The serial cultivation of human diploid cell strains. *Exp Cell Res* 25:585–621.
2. Bodnar AG, et al. (1998) Extension of life-span by introduction of telomerase into normal human cells. *Science* 279(5349):349–352.
3. Serrano M, Lin AW, McCurrach ME, Beach D, Lowe SW (1997) Oncogenic ras provokes premature cell senescence associated with accumulation of p53 and p16INK4a. *Cell* 88(5):593–602.
4. Rodier F, et al. (2009) Persistent DNA damage signalling triggers senescence-associated inflammatory cytokine secretion. *Nat Cell Biol* 11(8):973–979.
5. Coppé JP, et al. (2008) Senescence-associated secretory phenotypes reveal cell-nonautonomous functions of oncogenic RAS and the p53 tumor suppressor. *PLoS Biol* 6(12):2853–2868.
6. Kuilman T, Peeper DS (2009) Senescence-messaging secretome: SMS-ing cellular stress. *Nat Rev Cancer* 9(2):81–94.
7. Brack AS, et al. (2007) Increased Wnt signaling during aging alters muscle stem cell fate and increases fibrosis. *Science* 317(5839):807–810.
8. Krtolica A, et al. (2011) GROα regulates human embryonic stem cell self-renewal or adoption of a neuronal fate. *Differentiation* 81(4):222–232.
9. Pricola KL, Kuhn NZ, Haleem-Smith H, Song Y, Tuan RS (2009) Interleukin-6 maintains bone marrow-derived mesenchymal stem cell stemness by an ERK1/2-dependent mechanism. *J Cell Biochem* 108(3):577–588.
10. Krizhanovsky V, et al. (2008) Senescence of activated stellate cells limits liver fibrosis. *Cell* 134(4):657–667.
11. Xue W, et al. (2007) Senescence and tumour clearance is triggered by p53 restoration in murine liver carcinomas. *Nature* 445(7128):656–660.
12. Lawless C, et al. (2010) Quantitative assessment of markers for cell senescence. *Exp Gerontol* 45(10):772–778.
13. van Deursen JM (2014) The role of senescent cells in ageing. *Nature* 509(7501):439–446.
14. Kang C, et al. (2015) The DNA damage response induces inflammation and senescence by inhibiting autophagy of GATA4. *Science* 349(6255):aaa5612.
15. Sagiv A, Krizhanovsky V (2013) Immunosurveillance of senescent cells: The bright side of the senescence program. *Biogerontology* 14(6):617–628.
16. Grönwall C, Vas J, Silverman GJ (2012) Protective roles of natural IgM antibodies. *Front Immunol* 3:66.
17. Vas J, Grönwall C, Silverman GJ (2013) Fundamental roles of the innate-like repertoire of natural antibodies in immune homeostasis. *Front Immunol* 4:4.
18. Panda S, Ding JL (2015) Natural antibodies bridge innate and adaptive immunity. *J Immunol* 194(1):13–20.
19. Lutz HU, Binder CJ, Kaveri S (2009) Naturally occurring auto-antibodies in homeostasis and disease. *Trends Immunol* 30(1):43–51.
20. Grönwall C, et al. (2012) IgM autoantibodies to distinct apoptosis-associated antigens correlate with protection from cardiovascular events and renal disease in patients with SLE. *Clin Immunol* 142(3):390–398.
21. Lujambio A, et al. (2013) Non-cell-autonomous tumor suppression by p53. *Cell* 153(2):449–460.
22. Shimizu S, Sugai S, Konda S, Yamanaka Y, Setoyama M (1986) A monoclonal surface immunoglobulin (IgM/D-L) with specificity for surface antigen of ox red blood cells in a patient with leukemic lymphosarcoma. *J Clin Immunol* 6(5):397–401.
23. Satelli A, Li S (2011) Vimentin in cancer and its potential as a molecular target for cancer therapy. *Cell Mol Life Sci* 68(18):3033–3046.
24. Binder CJ (2012) Naturally occurring IgM antibodies to oxidation-specific epitopes. *Adv Exp Med Biol* 750:2–13.
25. Pastan I, et al. (1993) PR1—A monoclonal antibody that reacts with an antigen on the surface of normal and malignant prostate cells. *J Natl Cancer Inst* 85(14):1149–1154.
26. Inagaki T, et al. (1993) [Effective removal of the contaminating host fibroblasts for establishment of human-tumor cultured lines]. *Hum Cell* 6(2):137–142. Japanese.
27. Tsiantoulas D, Diehl CJ, Witztum JL, Binder CJ (2014) B cells and humoral immunity in atherosclerosis. *Circ Res* 114(11):1743–1756.
28. Belmokhtar CA, Hillion J, Ségal-Bendirdjian E (2001) Staurosporine induces apoptosis through both caspase-dependent and caspase-independent mechanisms. *Oncogene* 20(26):3354–3362.
29. Shaw PX, et al. (2000) Natural antibodies with the T15 idiotype may act in atherosclerosis, apoptotic clearance, and protective immunity. *J Clin Invest* 105(12):1731–1740.
30. Chou MY, et al. (2009) Oxidation-specific epitopes are dominant targets of innate natural antibodies in mice and humans. *J Clin Invest* 119(5):1335–1349.
31. Amir S, et al. (2012) Peptide mimotopes of malondialdehyde epitopes for clinical applications in cardiovascular disease. *J Lipid Res* 53(7):1316–1326.
32. Tuominen A, et al. (2006) A natural antibody to oxidized cardiolipin binds to oxidized low-density lipoprotein, apoptotic cells, and atherosclerotic lesions. *Arterioscler Thromb Vasc Biol* 26(9):2096–2102.
33. Esterre P, Melin M, Serrar M, Grimaud JA (1992) New specific markers of human and mouse fibroblasts. *Cell Mol Biol* 38(3):297–301.
34. Nishio K, Inoue A, Qiao S, Kondo H, Mimura A (2001) Senescence and cytoskeleton: Overproduction of vimentin induces senescent-like morphology in human fibroblasts. *Histochem Cell Biol* 116(4):321–327.
35. Chen C, Stenzel-Poore MP, Rittenberg MB (1991) Natural auto- and polyreactive antibodies differing from antigen-induced antibodies in the H chain CDR3. *J Immunol* 147(7):2359–2367.
36. Tsiantoulas D, et al. (2015) Circulating microparticles carry oxidation-specific epitopes and are recognized by natural IgM antibodies. *J Lipid Res* 56(2):440–448.
37. Horkovics-Kovats S, Traub P (1990) Specific interaction of the intermediate filament protein vimentin and its isolated N-terminus with negatively charged phospholipids as determined by vesicle aggregation, fusion, and leakage measurements. *Biochemistry* 29(37):8652–8657.
38. Perides G, Harter C, Traub P (1987) Electrostatic and hydrophobic interactions of the intermediate filament protein vimentin and its amino terminus with lipid bilayers. *J Biol Chem* 262(28):13742–13749.

39. Bilalic S, et al. (2012) Lymphocyte activation induces cell surface expression of an immunogenic vimentin isoform. *Transpl Immunol* 27(2-3):101–106.
40. Huet D, et al. (2006) SC5 mAb represents a unique tool for the detection of extracellular vimentin as a specific marker of Sezary cells. *J Immunol* 176(1):652–659.
41. Mitra A, et al. (2015) Cell-surface vimentin: A mislocalized protein for isolating csVimentin(+) CD133(-) novel stem-like hepatocellular carcinoma cells expressing EMT markers. *Int J Cancer* 137(2):491–496.
42. Mor-Vaknin N, Punturieri A, Sitwala K, Markovitz DM (2003) Vimentin is secreted by activated macrophages. *Nat Cell Biol* 5(1):59–63.
43. Moisan E, Girard D (2006) Cell surface expression of intermediate filament proteins vimentin and lamin B1 in human neutrophil spontaneous apoptosis. *J Leukoc Biol* 79(3):489–498.
44. Kueper T, et al. (2007) Vimentin is the specific target in skin glycation. Structural prerequisites, functional consequences, and role in skin aging. *J Biol Chem* 282(32):23427–23436.
45. Pamplona R, et al. (2005) Proteins in human brain cortex are modified by oxidation, glycoxidation, and lipoxidation. Effects of Alzheimer disease and identification of lipoxidation targets. *J Biol Chem* 280(22):21522–21530.
46. Spurny R, et al. (2007) Oxidation and nitrosylation of cysteines proximal to the intermediate filament (IF)-binding site of plectin: Effects on structure and vimentin binding and involvement in IF collapse. *J Biol Chem* 282(11):8175–8187.
47. Rogers KR, Morris CJ, Blake DR (1991) Oxidation of thiol in the vimentin cytoskeleton. *Biochem J* 275(Pt 3):789–791.
48. Pérez-Sala D, et al. (2015) Vimentin filament organization and stress sensing depend on its single cysteine residue and zinc binding. *Nat Commun* 6:7287.
49. Garzón B, Oeste CL, Díez-Dacal B, Pérez-Sala D (2011) Proteomic studies on protein modification by cyclopentenone prostaglandins: Expanding our view on electrophile actions. *J Proteomics* 74(11):2243–2263.
50. Traub P, Perides G, Kühn S, Scherbarth A (1987) Efficient interaction of nonpolar lipids with intermediate filaments of the vimentin type. *Eur J Cell Biol* 43(1):55–64.
51. Bhattacharya R, et al. (2009) Recruitment of vimentin to the cell surface by beta3 integrin and plectin mediates adhesion strength. *J Cell Sci* 122(Pt 9):1390–1400.
52. Morley JE, Farr SA, Kumar VB, Armbrecht HJ (2012) The SAMP8 mouse: A model to develop therapeutic interventions for Alzheimer's disease. *Curr Pharm Des* 18(8):1123–1130.
53. He XL, Zhou WQ, Bi MG, Du GH (2010) Neuroprotective effects of icariin on memory impairment and neurochemical deficits in senescence-accelerated mouse prone 8 (SAMP8) mice. *Brain Res* 1334:73–83.
54. Akbor MM, et al. (2013) Possible involvement of Hcn1 ion channel in learning and memory dysfunction in SAMP8 mice. *Biochem Biophys Res Commun* 441(1):25–30.
55. Nomura Y, Okuma Y (1999) Age-related defects in lifespan and learning ability in SAMP8 mice. *Neurobiol Aging* 20(2):111–115.
56. Tomobe K, Nomura Y (2009) Neurochemistry, neuropathology, and heredity in SAMP8: A mouse model of senescence. *Neurochem Res* 34(4):660–669.
57. Tomobe K, Shinozuka T, Kawashima T, Kawashima-Ohya Y, Nomura Y (2013) Age-related changes of forkhead transcription factor FOXO1 in the liver of senescence-accelerated mouse SAMP8. *Arch Gerontol Geriatr* 57(3):417–422.
58. Tomobe K, Shinozuka T, Kuroiwa M, Nomura Y (2012) Age-related changes of Nrf2 and phosphorylated GSK-3β in a mouse model of accelerated aging (SAMP8). *Arch Gerontol Geriatr* 54(2):e1–e7.
59. Cuesta S, et al. (2010) Melatonin improves inflammation processes in liver of senescence-accelerated prone male mice (SAMP8). *Exp Gerontol* 45(12):950–956.
60. Crisby M, Henareh L, Agewall S (2014) Relationship between oxidized LDL, IgM, and IgG autoantibodies to ox-LDL levels with recurrent cardiovascular events in Swedish patients with previous myocardial infarction. *Angiology* 65(10):932–936.
61. van Leeuwen M, et al. (2009) The IgM response to modified LDL in experimental atherosclerosis: hypochlorite-modified LDL IgM antibodies versus classical natural T15 IgM antibodies. *Ann N Y Acad Sci* 1173:274–279.
62. Su J, et al. (2006) Antibodies of IgM subclass to phosphorylcholine and oxidized LDL are protective factors for atherosclerosis in patients with hypertension. *Atherosclerosis* 188(1):160–166.
63. Ravandi A, et al. (2011) Relationship of IgG and IgM autoantibodies and immune complexes to oxidized LDL with markers of oxidation and inflammation and cardiovascular events: Results from the EPIC-Norfolk Study. *J Lipid Res* 52(10):1829–1836.
64. Garrido-Sánchez L, Chinchurreta P, García-Fuentes E, Mora M, Tinahones FJ (2010) A higher level of IgM anti-oxidized LDL antibodies is associated with a lower severity of coronary atherosclerosis in patients on statins. *Int J Cardiol* 145(2):263–264.
65. de Faire U, et al. (2010) Low levels of IgM antibodies to phosphorylcholine predict cardiovascular disease in 60-year old men: Effects on uptake of oxidized LDL in macrophages as a potential mechanism. *J Autoimmun* 34(2):73–79.
66. Klein-Schneegans AS, Kuntz L, Trembleau S, Fonteneau P, Loor F (1990) Serum concentrations of IgM, IgG1, IgG2b, IgG3 and IgA in C57BL/6 mice and their congenics at the nu(nude)locus. *Thymus* 16(1):45–54.
67. Singer KH, et al. (1989) Removal of fibroblasts from human epithelial cell cultures with use of a complement fixing monoclonal antibody reactive with human fibroblasts and monocytes/macrophages. *J Invest Dermatol* 92(2):166–170.
68. Jackson KJ, et al. (2012) Divergent human populations show extensive shared IGK rearrangements in peripheral blood B cells. *Immunogenetics* 64(1):3–14.
69. Hardy RR (2006) B-1 B cell development. *J Immunol* 177(5):2749–2754.
70. Ochsenbein AF, et al. (1999) Control of early viral and bacterial distribution and disease by natural antibodies. *Science* 286(5447):2156–2159.
71. deCathelineau AM, Henson PM (2003) The final step in programmed cell death: Phagocytes carry apoptotic cells to the grave. *Essays Biochem* 39:105–117.
72. Shaw PX, Goodyear CS, Chang MK, Witztum JL, Silverman GJ (2003) The autoreactivity of anti-phosphorylcholine antibodies for atherosclerosis-associated neoantigens and apoptotic cells. *J Immunol* 170(12):6151–6157.
73. Litvack ML, et al. (2010) Natural IgM and innate immune collectin SP-D bind to late apoptotic cells and enhance their clearance by alveolar macrophages in vivo. *Mol Immunol* 48(1-3):37–47.
74. Litvack ML, Post M, Palaniyar N (2011) IgM promotes the clearance of small particles and apoptotic microparticles by macrophages. *PLoS One* 6(3):e17223.
75. Starr AE, Bellac CL, Dufour A, Goebeler V, Overall CM (2012) Biochemical characterization and N-terminomics analysis of leukolysin, the membrane-type 6 matrix metalloprotease (MMP25): Chemokine and vimentin cleavages enhance cell migration and macrophage phagocytic activities. *J Biol Chem* 287(16):13382–13395.
76. Boilard E, Bourgoin SG, Bernatchez C, Surette ME (2003) Identification of an autoantigen on the surface of apoptotic human T cells as a new protein interacting with inflammatory group IIA phospholipase A2. *Blood* 102(8):2901–2909.
77. Ise H, Goto M, Komura K, Akaike T (2012) Engulfment and clearance of apoptotic cells based on a GlcNAc-binding lectin-like property of surface vimentin. *Glycobiology* 22(6):788–805.
78. Chen Y, Park YB, Patel E, Silverman GJ (2009) IgM antibodies to apoptosis-associated determinants recruit C1q and enhance dendritic cell phagocytosis of apoptotic cells. *J Immunol* 182(10):6031–6043.
79. Kofler R, Dixon FJ, Theofilopoulos AN (1987) The genetic origin of autoantibodies. *Immunol Today* 8(12):374–380.
80. Leibundgut G, et al. (2012) Oxidized phospholipids are present on plasminogen, affect fibrinolysis, and increase following acute myocardial infarction. *J Am Coll Cardiol* 59(16):1426–1437.
81. Oeste CL, Pérez-Sala D (2014) Modification of cysteine residues by cyclopentenone prostaglandins: Interplay with redox regulation of protein function. *Mass Spectrom Rev* 33(2):110–125.
82. Gharbi S, Garzón B, Gayarre J, Timms J, Pérez-Sala D (2007) Study of protein targets for covalent modification by the antitumoral and anti-inflammatory prostaglandin PGA1: Focus on vimentin. *J Mass Spectrom* 42(11):1474–1484.
83. Hong SH, et al. (2006) Identification of a specific vimentin isoform that induces an antibody response in pancreatic cancer. *Biomark Insights* 1:175–183.
84. Satelli A, Brownlee Z, Mitra A, Meng QH, Li S (2015) Circulating tumor cell enumeration with a combination of epithelial cell adhesion molecule- and cell-surface vimentin-based methods for monitoring breast cancer therapeutic response. *Clin Chem* 61(1):259–266.
85. Satelli A, et al. (2014) Universal marker and detection tool for human sarcoma circulating tumor cells. *Cancer Res* 74(6):1645–1650.
86. Darvin K, et al. (2014) Plasma protein biomarkers of the geriatric syndrome of frailty. *J Gerontol A Biol Sci Med Sci* 69(2):182–186.
87. Shamsi KS, et al. (2012) Proteomic screening of glycoproteins in human plasma for frailty biomarkers. *J Gerontol A Biol Sci Med Sci* 67(8):853–864.
88. Tanisawa K, et al. (2013) Exome sequencing of senescence-accelerated mice (SAM) reveals deleterious mutations in degenerative disease-causing genes. *BMC Genomics* 14:248.
89. Smith CG, et al. (2013) Role of the oxidative DNA damage repair gene OGG1 in colorectal tumorigenesis. *J Natl Cancer Inst* 105(16):1249–1253.
90. Smith TB, et al. (2013) The presence of a truncated base excision repair pathway in human spermatozoa that is mediated by OGG1. *J Cell Sci* 126(Pt 6):1488–1497.
91. Choi JY, et al. (1999) Thermolabile 8-hydroxyguanine DNA glycosylase with low activity in senescence-accelerated mice due to a single-base mutation. *Free Radic Biol Med* 27(7-8):848–854.
92. Zhu JK (2009) Active DNA demethylation mediated by DNA glycosylases. *Annu Rev Genet* 43:143–166.
93. Krokan HE, et al. (2014) Error-free versus mutagenic processing of genomic uracil—Relevance to cancer. *DNA Repair (Amst)* 19:38–47.
94. Baker DJ, et al. (2004) BubR1 insufficiency causes early onset of aging-associated phenotypes and infertility in mice. *Nat Genet* 36(7):744–749.
95. Kapanidou M, Lee S, Bolanos-Garcia VM (2015) BubR1 kinase: Protection against aneuploidy and premature aging. *Trends Mol Med* 21(6):364–372.
96. Salminen A, et al. (2011) Astrocytes in the aging brain express characteristics of senescence-associated secretory phenotype. *Eur J Neurosci* 34(1):3–11.
97. Gan W, et al. (2012) Age-dependent increases in the oxidative damage of DNA, RNA, and their metabolites in normal and senescence-accelerated mice analyzed by LC-MS/MS: Urinary 8-oxoguanosine as a novel biomarker of aging. *Free Radic Biol Med* 52(9):1700–1707.
98. Miller YI, Tsimikas S (2013) Oxidation-specific epitopes as targets for biotheranostic applications in humans: Biomarkers, molecular imaging and therapeutics. *Curr Opin Lipidol* 24(5):426–437.
99. Fruhwirth GO, Loidl A, Hermetter A (2007) Oxidized phospholipids: From molecular properties to disease. *Biochim Biophys Acta* 1772(7):718–736.
100. Holt PG, et al. (1985) Preparation of interstitial lung cells by enzymatic digestion of tissue slices: Preliminary characterization by morphology and performance in functional assays. *Immunology* 54(1):139–147.
101. Lyadova I, et al. (1998) An ex vivo study of T lymphocytes recovered from the lungs of I/St mice infected with and susceptible to *Mycobacterium tuberculosis*. *Infect Immun* 66(10):4981–4988.
102. Baglole CJ, et al. (2005) Isolation and phenotypic characterization of lung fibroblasts. *Methods Mol Med* 117:115–127.
103. Seluanov A, Vaidya A, Gorbunova V (2010) Establishing primary adult fibroblast cultures from rodents. *J Vis Exp* (44):2033.
104. Kapina MA, Rubakova EI, Majorov KB, Logunova NN, Apt AS (2013) Capacity of lung stroma to educate dendritic cells inhibiting mycobacteria-specific T-cell response depends upon genetic susceptibility to tuberculosis. *PLoS One* 8(8):e72773.
105. Di Leonardo A, Linke SP, Clarkin K, Wahl GM (1994) DNA damage triggers a prolonged p53-dependent G1 arrest and long-term induction of Cip1 in normal human fibroblasts. *Genes Dev* 8(21):2540–2551.
106. Aoshiba K, Tsuji T, Nagai A (2003) Bleomycin induces cellular senescence in alveolar epithelial cells. *Eur Respir J* 22(3):436–443.
107. Frescas D, Guardavaccaro D, Bassermann F, Koyama-Nasu R, Pagano M (2007) JHDM1B/FBXL10 is a nucleolar protein that represses transcription of ribosomal RNA genes. *Nature* 450(7167):309–313.
108. Xu B, et al. (2004) The endothelial cell-specific antibody PAL-E identifies a secreted form of vimentin in the blood vasculature. *Mol Cell Biol* 24(20):9198–9206.